How to cite: *Angew. Chem. Int. Ed.* **2024**, *63*, e202314773
doi.org/10.1002/anie.202314773

Micellar Catalysis

Molecular Dynamic Simulations of Aqueous Micellar Organometallic Catalysis: Methane Functionalization as a Case Study

Alejandra Matamoros-Recio, Elia Alonso-Rueda, Elena Borrego, Ana Caballero, Pedro J. Pérez,* and Sonsoles Martín-Santamaría**

In memory of Professor Gregorio Asensio.

Abstract: Molecular Dynamics (MD) simulations constitute a powerful tool that provides a 3D perspective of the dynamical behavior of chemical systems. Herein the first MD study of the dynamics of a catalytic organometallic system, in micellar media, is presented. The challenging methane catalytic functionalization into ethyl propionate through a silver-catalyzed process has been targeted as the case study. The intimate nature of the micelles formed with the surfactants sodium dodecylsulfate (SDS) and potassium perfluorooctane sulfonate (PFOS) has been ascertained, as well as the relative distribution of the main actors in this transformation, namely methane, the diazo reagent and the silver catalyst, the latter in two different forms: the initial compound and a silver-carbene intermediate. Catalyst deactivation occurs with halide containing surfactants dodecyltrimethylammonium chloride (DTAC) and Triton X-100. Computed simulations allow explaining the experimental results, indicating that micelles behave differently regarding the degree of accumulation and the local distribution of the reactants and their effect in the molecular collisions leading to net reaction.

Introduction

Among the well-known twelve principles of green chemistry,[1] the use of safer solvents (principle #5) and catalytic methods (principle #9) are currently the focus of a plethora of investigations. Replacing organic solvents, which originate a waste problem and involve energy cost at production, by a non-toxic, disposable and readily available reaction medium constitutes a must, nowadays.[2] Additionally, catalytic methods allow decreasing byproducts, also considered as waste.[3] However, many metal-based catalytic systems usually operate at loadings that are yet higher than those desired in terms of metal supply at the long-term.[4]

[*] Dr. A. Matamoros-Recio, E. Alonso-Rueda, Dr. S. Martín-Santamaría
Department of Structural and Chemical Biology, Centro de Investigaciones Biológicas Margarita Salas (CSIC)
28040 Madrid (Spain)
E-mail: smsantamaria@cib.csic.es
Dr. E. Borrego, Dr. A. Caballero, Prof. Dr. P. J. Pérez
Laboratorio de Catálisis Homogénea, Unidad Asociada al CSIC, CIQSO-Centro de Investigación en Química Sostenible and Departamento de Química, Universidad de Huelva
21007 Huelva (Spain)
E-mail: ana.caballero@dqcm.uhu.es
perez@dqcm.uhu.es

In the context of green chemistry, and the need of more sustainable processes, aqueous micellar catalysis[5] has emerged in this century as a tool for accomplishing organic transformations, in a catalytic manner, providing certain improvements related to the use of safer solvents and catalysts. This methodology is based on the formation of molecular aggregates in water from amphiphilic molecules (surfactants), which undergo a process of self-aggregation leading to the formation of species which can incorporate catalysts and reactants inside, acting as a nanoreactor (Scheme 1a).[6] This accumulation of the actors of the chemical reaction in such small volume triggers the transformation, avoiding the use of heating and also favoring catalyst loadings lower than those employed in organic solvents.

The above strategy has been developed with great success in the last decades, particularly boosted by the group of Lipshutz,[7–9] which has developed a number of catalytic transformations in aqueous micellar catalysis under very mild conditions and decreasing substantially the E-factor (as a measurement of the waste generated by a process).[10] Most of their findings are based on the use of TPGS-750-M as the surfactant, and their success has already been transferred to industry.[11,12]

Despite the utility of this strategy, little efforts have been devoted to the knowledge of the interaction of the catalysts, reactants and products within the micelle, and/or the micelle and the water medium. Models have been applied from a kinetic point of view to explain the reactivity in emulsions.[13] Very recently, Andersson has reported on how the micelles generated from TPGS-750-M organize themselves, using density functional theory and the COS-

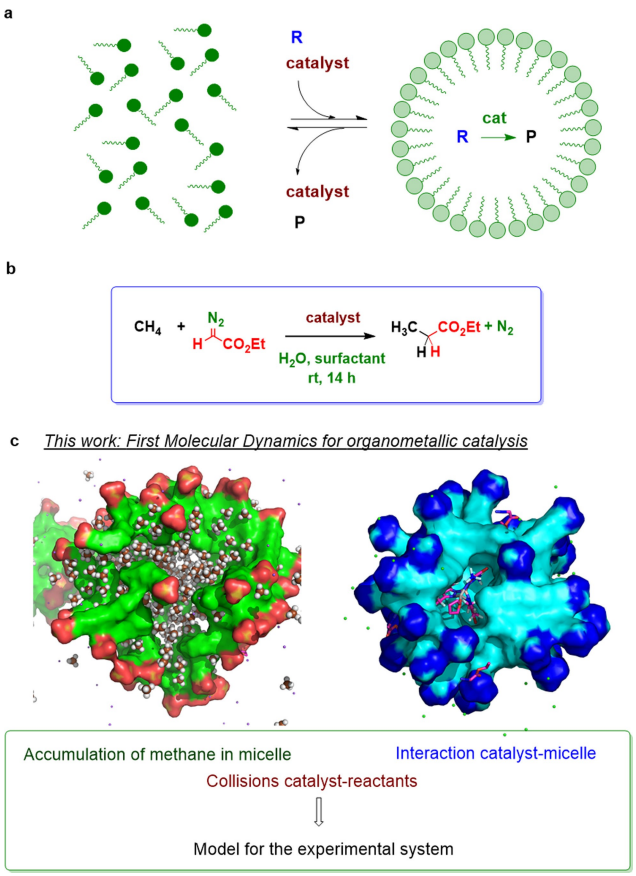

Scheme 1. Introducing Molecular Dynamics (MD) simulations to organometallic catalysis. **A**, General, simple view of micellar catalysis. **B**, The case study of methane functionalization by carbene transfer from a diazo compound catalyzed by silver in micellar media. **c**, MD simulations of this transformation, from which the accumulation of reactants (methane, diazo compound), the catalyst (in different species) and the collisions among them are modeled, fitting the experimental results.

MO-RS implicit solvent model.[14] He has also correlated the increase of reaction rates in micellar catalysis with the decrease of entropy.[15] However, to the best of our knowledge, there are no studies for micellar catalysis to explain not only the accumulation of catalyst and reactants inside the nanoreactor but also the effect of the micelle on reaction intermediates and, subsequently, in the reaction outcome. Molecular Dynamics (MD) simulations can reveal information about interaction properties and behavior of atoms and molecules, where experimental techniques are often not applicable, and provide the 3D perspective of the dynamical behavior and properties of surfactant molecules and their aggregates. For this reason, MD simulations have been used to investigate the dynamics and self-assembly of several types of surfactant solutions, and to analyze micelle formation of surfactants with different structural and physicochemical properties, either by all-atom or coarse-grained MD approaches.[16–19] MD simulations have also been employed in the study of the efficiency of surfactant aggregates to encapsulate molecules, with special focus on drugs and peptides, for which MD simulations can accurately reproduce experimental ensemble averages, partition coefficients, and diffusion constants, unraveling the molecular mechanisms of surfactants encapsulation efficiency.[20]

On the other hand, MD simulations have also proven to be a useful tool for gaining microscopic insights into chemical reactions, including catalytic processes. MD simulations of reactants and/or reaction intermediates under experimental conditions can provide relevant details about the effect of the surrounding medium on the reaction yields.[21] For example, MD simulations of catalytic intermediates in enzyme active sites have been successfully applied to unveil the role of intermediates distribution and the effect of the charge and hydrophobicity of the enzyme active site in generating a suitable environment for catalytic reactions.[22]

We have recently communicated on the catalytic functionalization of methane employing micellar catalysis (Scheme 1b).[23] This was the first example of methane being functionalized in water at room temperature, where we hypothesized that aggregates from surfactants act as methane concentrators also trapping the catalyst (the silver complex $Tp^{(CF3)2,Br}Ag(thf)$) and the diazo reagent. In addition, the reaction pathway for this type of transformation has been previously modeled by MM and DFT.[24] Based on the information gathered in these previous studies, and novel experimental data reported herein, we now provide the first study of the dynamics of an organometallic catalytic system under aqueous micellar conditions (Scheme 1c), by means of all-atom MD simulations, using the above methane functionalization reaction as the probe transformation. We aimed at exploring the structural properties of the micelles and the interatomic interactions within the micellar systems, for a more comprehensive understanding of the micellar catalytic reaction. Several features such as the effect of the nature of the surfactant in micelle generation, catalysts and reactants accumulation, and the interaction of intermediates with the micelles have been clarified based on the computational simulations. Overall, the understanding of this micellar catalytic system through MD studies explains the differences experimentally observed with the series of surfactant employed, which are due to the aforementioned several variables.

Results and Discussion

Methane functionalization by micellar catalysis

The catalytic functionalization of methane by metal-catalyzed carbene transfer reaction from a diazo compound was first disclosed by one of our groups in 2011,[25] employing supercritical carbon dioxide as the reaction medium. With this strategy, the C–H bonds of methane find no other carbon-hydrogen bonds in the reaction vessel, therefore eliminating competition pathways. After this work, and with the same idea in mind, we decided to move onto aqueous micellar catalysis, aiming at concentrating methane, the diazo compound and the catalyst inside the micelle formed by the surfactants. A preliminary communication on these

results has been disclosed, albeit some new and relevant experimental data are now herein provided.[23]

First, the trapping of methane by micelles was investigated, and the amount of CH_4 retained in the aqueous solution of the surfactant was quantified employing five representative members: sodium dodecylsulfate (SDS), dodecyltrimethylammonium chloride (DTAC), Triton X-100, TPGS-750-M and potassium perfluorooctane sulfonate (PFOS). Scheme 2a shows the variation of the [CH_4] (mM) in solution with the concentration of surfactant, obtained upon exposing of the micelle solution under 160 bar of methane at room temperature. A similar behavior was observed in all cases, the amount of methane reaching maxima within the range of 100–300 mM of the surfactant, in all cases the critical micellar concentration being surpassed. Maxima values of [CH_4] ranged from 320 mM (PFOS) to 2200 mM, i.e. 2.2 M for Triton X-100. It is worth noting that the solubility of methane in water is very low, 2×10^{-5} molar fraction,[26] therefore the micelle trapping is effective, albeit largely dependent of the surfactant employed. Once verified that methane was accumulated in the micellar media, we run the corresponding catalytic experiments, where complex $Tp^{(CF3)2,Br}Ag(thf)$ was employed as the catalyst and ethyl diazoacetate (EDA) as the carbene precursor. Scheme 2b displays the results obtained for the reactions carried out at room temperature, with distinct outcome. Both Triton X-100 and DTAC were not effective towards catalysis, despite their capabilities toward methane accumulation. Lipshutz's surfactant, TPGS-750-M, gave only 2 % of ethyl propionate, whereas micelles derived from SDS

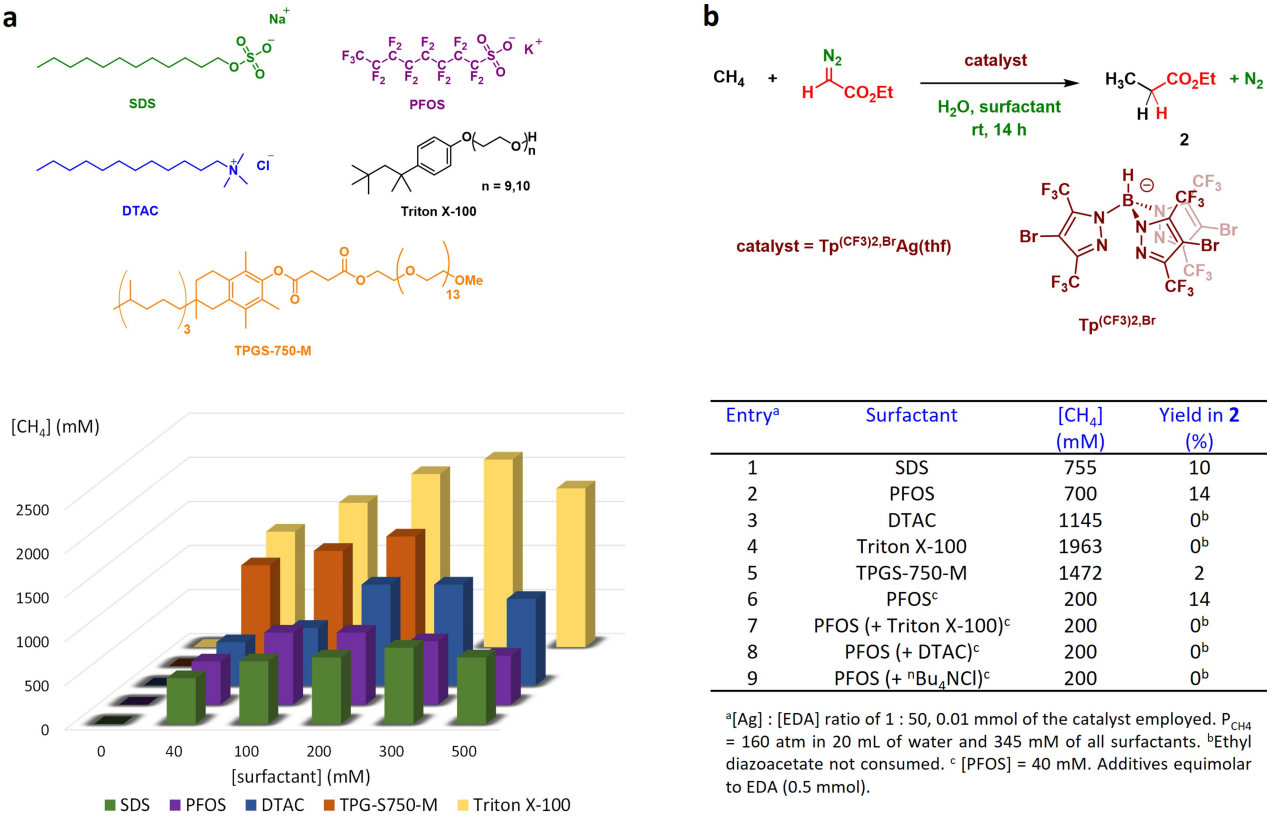

Entry[a]	Surfactant	[CH_4] (mM)	Yield in **2** (%)
1	SDS	755	10
2	PFOS	700	14
3	DTAC	1145	0[b]
4	Triton X-100	1963	0[b]
5	TPGS-750-M	1472	2
6	PFOS[c]	200	14
7	PFOS (+ Triton X-100)[c]	200	0[b]
8	PFOS (+ DTAC)[c]	200	0[b]
9	PFOS (+ $^nBu_4NCl$)[c]	200	0[b]

[a][Ag] : [EDA] ratio of 1 : 50, 0.01 mmol of the catalyst employed. P_{CH4} = 160 atm in 20 mL of water and 345 mM of all surfactants. [b]Ethyl diazoacetate not consumed. [c] [PFOS] = 40 mM. Additives equimolar to EDA (0.5 mmol).

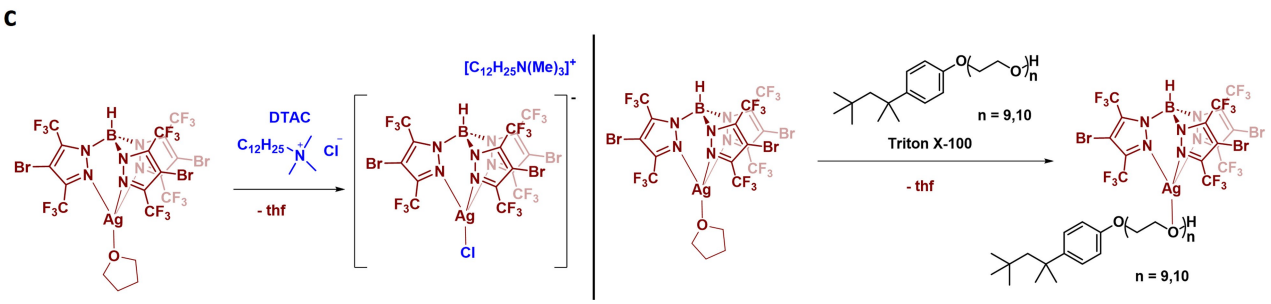

Scheme 2. Methane functionalization in water-surfactant media. **a**, Accumulation of methane (in mM) in the aqueous micelles generated by the surfactants at room temperature. **b**, Silver-catalyzed methane functionalization by carbene insertion from ethyl diazoacetate under micellar conditions. **c**, Catalyst deactivation by surfactants DTAC and Triton X-100.

and PFOS resulted more useful as nanoreactors since they led to 10 % and 14 % yield into ethyl propionate.

We further investigated the lack of catalytic activity when using Triton X-100 and DTAC as surfactants, where EDA remained unreacted after the reaction time, i.e., the catalyst was inactive in such reaction media. To collect information on this issue, we repeated the experiment carried out with PFOS with the incorporation of Triton X-100 and DTAC as additives, which led to inhibition of the catalytic reaction (Scheme 2b, entries 7–8). These results assess the existence of interactions between the silver catalyst and both surfactants that completely inhibit the reaction of the catalyst with ethyl diazoacetate. Literature reports support such proposal. Thus, the reaction of $AgNO_3$ with CTAB (cetyltrimethylammonium bromide), a surfactant similar to DTAC, has been reported[27] to produce a CTA–Ag–Br complex in which the silver center adds the bromide from the surfactant, and the cetyltrimethylammonium acts as the counterion. Based on this precedent, we propose that complex $Tp^{(CF3)2,Br}Ag(thf)$ undergoes reaction with DTAC, where the chloride ion blocks the coordination site of the silver center available for catalysis (Scheme 2c). To reinforce this proposal, another experiment in which $^{n}Bu_4NCl$ was added also showed catalyst inhibition (Scheme 2b, entry 9), demonstrating that such effect does not depend of the potential micelle formation of the additive (DTAC or $^{n}Bu_4NCl$).

For the Triton X-100 case, it has been reported the large affinity of Ag(I) ions to coordinate the ether groups of this surfactant,[28] thus blocking further interactions. Given that the $Tp^{x}Ag$ cores display a great affinity towards the oxygen donor atoms of thf or acetone, among others, and the large number of O-donors available in Triton X-100, we propose such coordination as responsible for the lack of catalytic activity of the silver complex when employed in micellar media with such surfactant (Scheme 2c). The same reactivity could explain the low yields obtained with TPGS-750-M: the presence of ether groups in their chains also favors coordination to silver. In this case, it is very likely that the coordination-decoordination equilibrium delivers accessible amounts of free silver catalyst to react with EDA.

From experimental data, given there is no correlation between the concentration of methane and the reaction yield, it is evident that the catalytic activity is influenced by the surfactant (SDS or PFOS) nature. In order to find explanations for the observed experimental behavior, we decided to study the time-evolution of this system in the different surfactant environments (micelles) by MD simulations with SDS and PFOS, since any simulation with DTAC o Triton X-100 would be not useful given that the catalyst is deactivated and **I1** is not formed.

Molecular Dynamics simulation studies

We focused our studies into silver complexes identified as relevant in previous DFT studies[24] (Scheme 3a). The catalyst precursor **I1** reacts with the diazo compound forming a silver-carbene intermediate **I4** in the rate determining step for this transformation, which further reacts with methane in an irreversible step. In order to explore the factors that control this transformation, we have performed computational studies of the catalyst **I1** and EDA reactant in the SDS and PFOS micelles in water, as well as the methane interaction with intermediate **I4**, in the same surfactants, since both promote the catalytic transformation at a substantial degree while other tested surfactants do not. We have also performed the simulations of the different surfactants mixtures to explain the formation of micelles, as well as the allocation of the reactants within the micelles. All the simulations protocols were set-up according to the experimental conditions of concentration, pressure and temperature, which were kept along the simulation (see Supporting Information).

Surfactant self-assembly

To study the behavior of the **I1** in the surfactants used experimentally, two simplistic systems were constructed, each of them consisting in a water cubic box of $(100\ Å)^3$, with 2 molecules of **I1**, 15 molecules of EDA, and 208 molecules of the corresponding surfactant, i.e., SDS or PFOS, and starting from random initial molecules positions (Scheme 3b,c). Systems were simulated during 1 μs, at 300 K and 1 bar. During the simulation time, spontaneous aggregation of the surfactants into micelles was observed (Scheme 3c). The micellization process along simulation time was illustrated by plotting the evolution of cluster number (Nclust), and the Solvent Accessible Surface Area (SASA) of the surfactant molecules, i.e., the surface area of the aggregates exposed or accessible to water (Scheme 3d,e). The formation of micelles occurred during the first 150 ns of simulation run for both the PFOS and SDS systems. Data showed that surfactant monomers surround the catalyst molecules from the beginning of the simulations in both, SDS and PFOS, forming a micelle around it over time. In the case of the PFOS system, the catalyst remains embedded into the micelle formed, whereas in the case of SDS, the surfactant molecules do not completely surround the catalyst, and one of its faces (the face pointing to the observer) remains exposed to the solvent (Figure S1).

SASA profiles decreased along the micellization period, and then, remained constant until the end of the simulations, pointing to a self-aggregation process by the tendency of surfactant molecules to protect their hydrophobic parts from water (Scheme 3e). To quantify this finding, we computed the Nclust and the average number of surfactant molecules per cluster, Nagg, during simulation time. As observed in Scheme 3d,e, the initially randomly placed monomers of surfactants first aggregated into small clusters and subsequently, these clusters self-assembled to form larger micelles. Thus, the Nclust decreases during the micellization period, and then remained almost constant (Scheme 3d). Accordingly, the Nagg followed the opposite trend (Figure S2). After micellization, the average Nclust fluctuated between 7 and 9 in SDS and 6 and 10 in PFOS. The formed micelles had a size (Nagg) of 23–29 monomers in SDS and

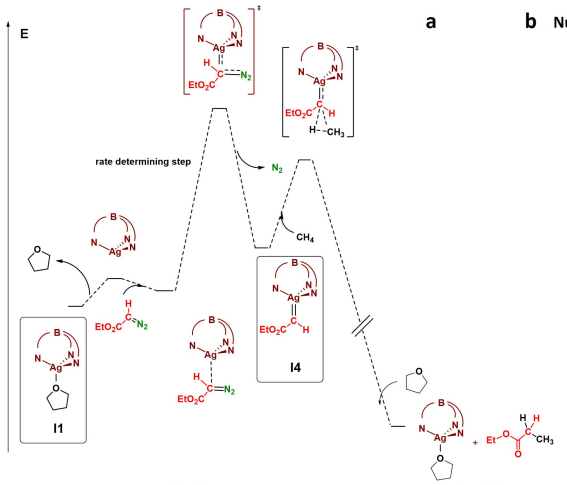

b Number of molecules in the simulated models, according to experimental concentrations

System	Surfactant and counterion[a]	Silver species	EDA	Methane	Water
	Concentration (mM)				
I1-Surfactant	345	0.016	25	—	—
I4-Surfactant	345	0.016	—	—	—
I4-Surfactant-methane	345	0.016	—	800 / 700[b]	—
	Number of molecules				
I1-Surfactant	208	2	15	—	33450
I4-Surfactant	208	2	—	—	33450
I4-Surfactant-methane	208	2	—	482 / 425[b]	33450

[a]Counterions are Na^+ in SDS, K^+ in PFOS. [b]Methane uptake (mM) at surfactant concentration of 345 mM is 800 mM in SDS and 700 mM in PFOS.

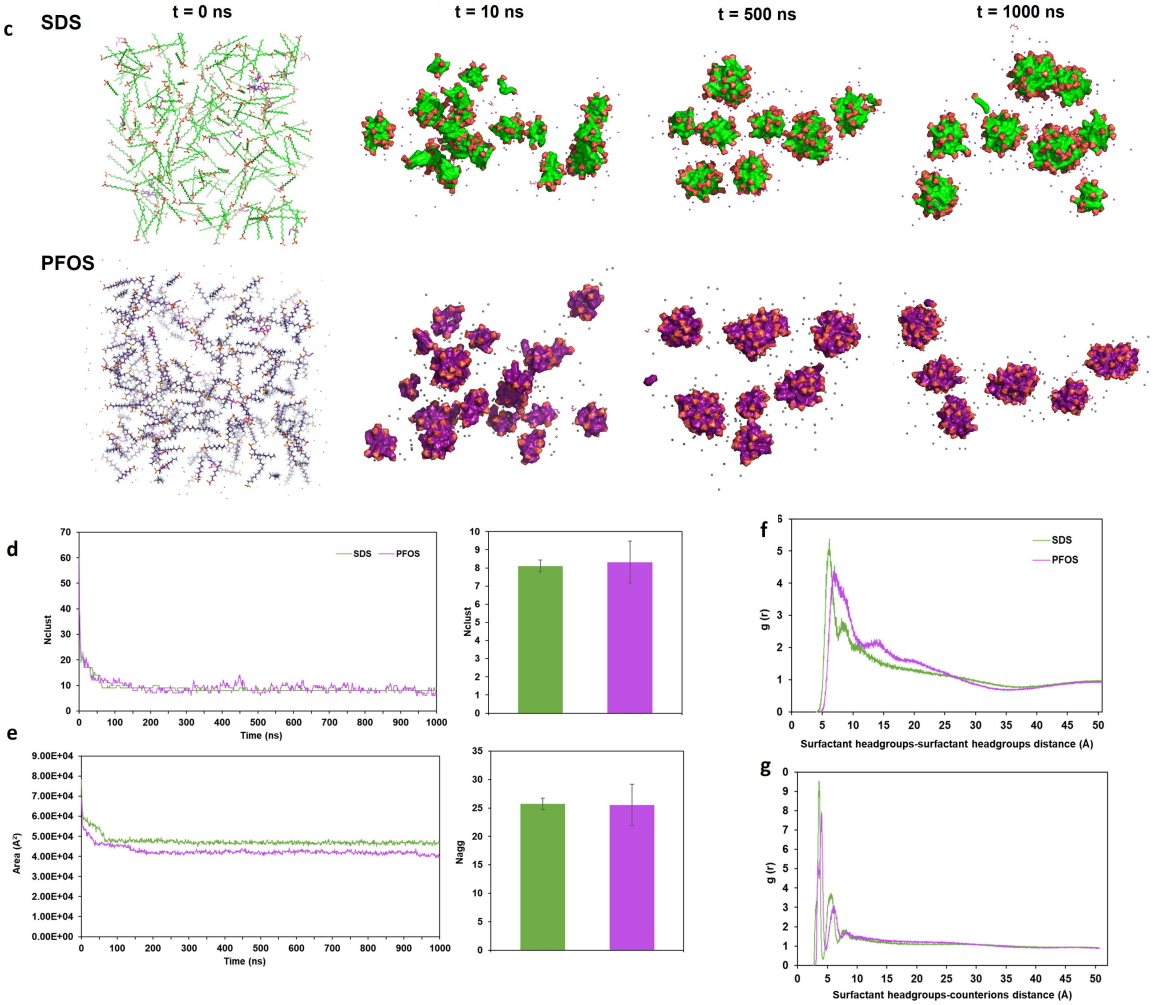

Scheme 3. MD simulation of micelle formation with SDS and PFOS and relevant catalytic species. **a**, DFT profile of the methane functionalization by carbene insertion with the silver catalyst $Tp^xAg(thf)$. **b**, Number of molecules in the simulated models, according to experimental concentrations. **c**, MD simulations (t = 1 μs) of the surfactant monomers with **I1** and ethyl diazoacetate in aqueous solution. Aggregation of surfactants into micelles is observed. Surfactants are represented as green (SDS), purple (PFOS), sticks in the 0 ns frame, and as surface in the rest of frames. See Figure 4 for expanded aggregates. Water molecules are hidden, for the sake of clarity. **d**, Number of clusters, Nclust, observed during the MD simulations of the **I1** with the surfactant models. **e**, Solvent accessible surface area (SASA) of surfactant molecules computed over MD simulation time (t = 1 μs). Values predicted Nclust and Nagg for the last 300 ns of simulation are plotted on the right, for a more detailed view. **f**, Radial distribution function, g(r), of the surfactant headgroups, and **g** radial distributions of counterions around the surfactant headgroups, during the last 300 ns of MD simulation in the **I1**-surfactant systems.

17–35 in PFOS (Scheme 3d,e and Figure S2). The variations in Nclust and Nagg values occur due to the disassembly of surfactant monomers from the surface of micelles, which subsequently reassemble to other micelles. In the cluster quantification, the monomers that travel through the aqueous medium from one micelle to another are quantified as one cluster. Therefore, this is not an adequate method to determine the exact number of micelles in each system but allows to determine which of the studied systems forms the most stable aggregates. As observed, SDS showed lower variations than PFOS, suggesting that the former assembled into the most stable micelles. Furthermore, the number of micelles formed in each system after the micellization period was determined by visual inspection. Observed values were 8 in SDS and 6 to 8 in PFOS.

For a deeper study of the structural properties of the micelles, we calculated the distribution of Nagg in the different systems, after stabilization (after 400 ns of simulation time). As observed in the corresponding histograms (Figure S2B), the formed micelles had sizes (Nagg) ranging from 13–46 monomers in SDS and 10–41 in PFOS, pointing to a polydisperse population in both systems. Remarkably, some of the predicted Nagg values are similar to those previously described in the literature, at close conditions to those studied here,[29,30] whereas others are smaller. Nevertheless, it is well known that the Nagg depends on several factors, such as surfactant concentration,[31] pH,[32] temperature,[33] solvent,[34] salt concentration,[35, 36] nature of counterions,[33] and, more importantly, the presence of additional molecules, such as cosurfactants[37] or other solutes.[38] On this basis, we can assume that the presence in our systems of EDA, methane and the catalyst intermediates, could lead to smaller micelles. Indeed, not all micelles are interacting with the same number of EDA, methane, and catalyst molecules. Particularly, due to the surfactant/catalyst ratio, some of the micelles do not interact with any catalyst molecule. Therefore, the effect of the reagents and the catalyst on the Nagg of the micelles will not be equal in all of them, which could explain the presence of several micelles with diverse Nagg (i.e., polydispersity). We must take into account the large amount of methane trapped within the micelles which should strongly affect the aggregation process.

To further characterize the formed micelles, we explored the interatomic interactions by calculating the radial distribution function, g(r), between surfactant headgroups (Scheme 3f). The g(r) describes the probability of finding a particle around a reference particle, as a function of distance (r). On this basis, the largest intensity peaks observed in the g(r) plots correspond to the closest and preferential localization of headgroup atoms together. Density values, g(r), of the largest peak predicted for the ionic surfactants were observed at 5.38 Å in SDS and 7.00 Å in PFOS (Scheme 3f). Since SDS exhibited its largest g(r) peak at the lowest distance (r), it could be suggested that the SDS ionic headgroups remained closer than the PFOS headgroups, and thus suffered less electrostatic repulsion.

The presence of oppositely charged ions attenuates the repulsion among the charged headgroups of ionic surfactants on the micelles surface of charged surfactants and ensure micelles stability. We analyzed the g(r), between each ionic surfactant headgroups and the corresponding ions, i.e., Na^+ in SDS and K^+ (Scheme 3g). As observed, the g(r) largest intensity peaks were predicted at 3.66 Å in SDS and 4.04 Å in PFOS. Clearly, SDS presented the lowest distance between surfactant headgroups and counterions. Moreover, the presence of a second g(r) peak in the SDS and PFOS systems indicates that both surfactants have high affinities to their counterions.[39] Therefore, Na^+ ion in the SDS system is a more efficient counterion, which could allow the formation of more stable micelles than in the PFOS system.

Accumulation of I1 and EDA in the micelles

Since we have experimentally demonstrated that reaction does not occur in water as solvent, the surfactant aggregates must concentrate reactants and catalyst in the concentrations and time required for the catalytic reaction. Data collected show (Scheme 4a) that **I1** molecules are completely buried inside the micelles core in the PFOS system and adsorbed on the SDS micelles surface with the coordinated tetrahydrofuran ligand pointing towards the water solvent. Therefore, **I1** is embedded to a lesser extent in SDS than in PFOS.

For a deeper analysis of the catalyst-micelles interactions, we analyzed the number of water molecules around the **I1** molecules during the MD simulations. As consequence of **I1** resulting internalized inside the PFOS system, a sharp drop was observed in the number of water molecules (Nwat) around **I1** molecules during the micellization process (Scheme 4b). On the other hand, the decrease was not evident in the SDS system, confirming that the **I1** molecules remained exposed to solvent all along the MD simulation time. At the end of the MD simulations, more water molecules surrounded the **I1** in the case of SDS than that of PFOS.

We also monitored the radial distributions g(r) based on the probability densities of surfactants polar headgroups around the **I1** molecules (Scheme 4c). The highest density peaks of the g(r) were located at 9.76 Å in SDS and 15.20 Å in PFOS. It is evident that the lowest value observed in the SDS system is due to the adsorption of the catalyst on the surfaces of the micelles, remaining close to the headgroups of the surfactants. On the other hand, distances were higher in the PFOS system since the catalyst molecules were embedded inside the micelles cores and become positioned further away from the headgroups (Scheme 4a). Our analyses show the greater ability of PFOS surfactant to embed the catalyst molecules inside the micellar interior and protect them from water exposition, compared to SDS in which the **I1** is adsorbed on the micelles surfaces and remains solvent exposed.

Regarding the ethyl diazoacetate (EDA) reagent, it was observed that the molecules remained on the surface of the micelles (Scheme 4a). According to the Nwat values, the EDA molecules were more exposed to the aqueous medium in SDS than in PFOS (Scheme 4d). These observations

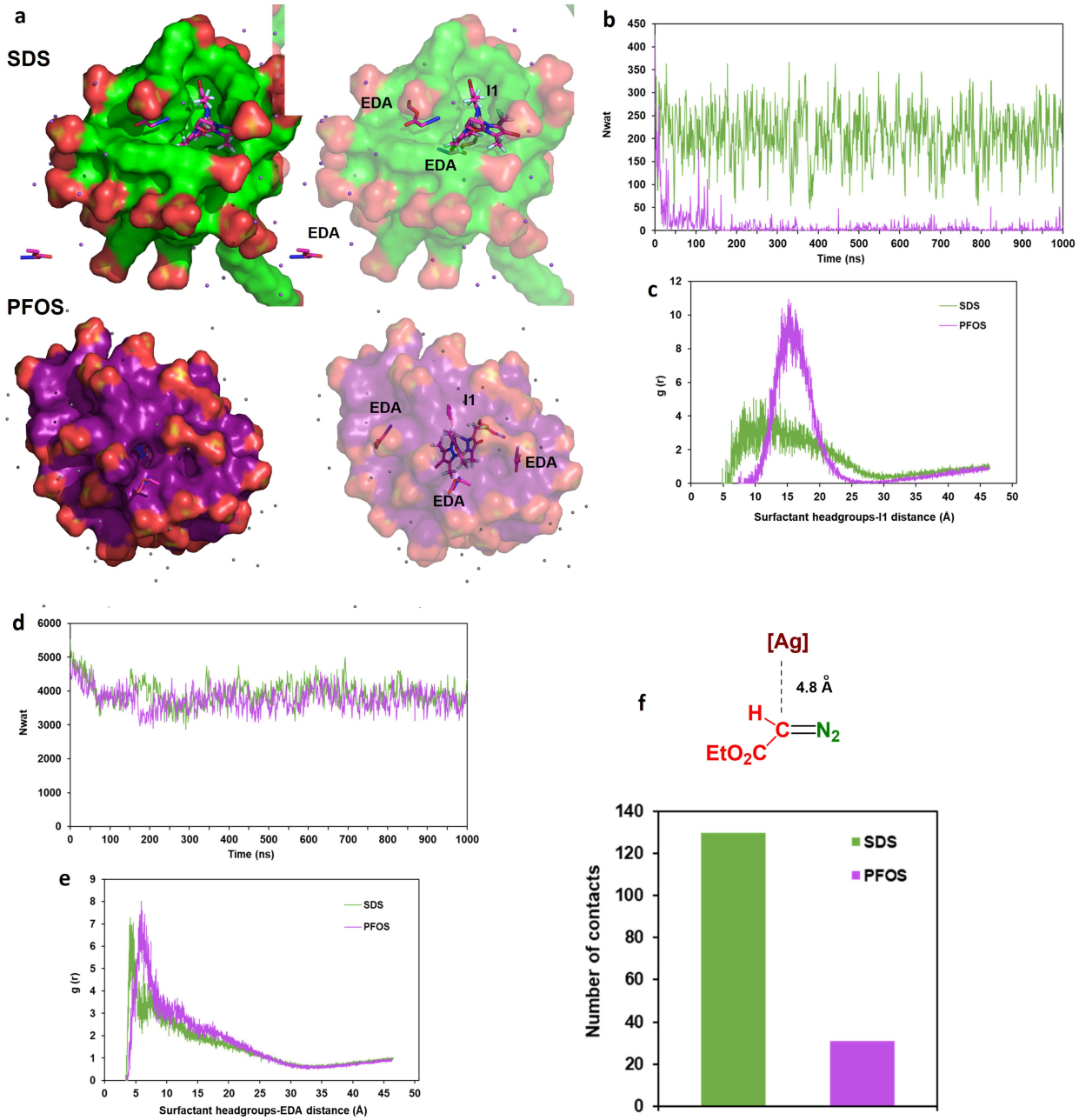

Scheme 4. MD simulation of **I1** and EDA in the micelles. **a**, Detailed view of the localization of **I1** and EDA localization in the micellar aggregates during MD simulations of the **I1**-Surfactant models. Surfactants are represented as green (SDS) and purple (PFOS), opaque surface on the left, and semi-transparent surface on the right. Water molecules and hydrogens are hidden for clarity. **b**, Number of water molecules surrounding **I1** molecules within 10 Å. **c**, Radial distribution, g(r), of the surfactant headgroups around **I1**. Radial distribution profiles were calculated during the last 300 ns of MD simulations. **d**, Number of molecules of water around the EDA molecules. **e**, Radial distribution values of surfactant headgroups to EDA molecules. Radial distribution profiles were calculated during the last 300 ns of MD simulations. **f**, Cumulative number of interactions between **I1** and ethyl diazoacetate molecules at a cutoff distance of 4.8 Å (distance chosen from DFT studies), as predicted for the last 300 ns of simulations in the two **I1**-surfactant models.

agreed with the g(r) plots calculated for the surfactants headgroups around the EDA, in which the largest density peaks were located at 4.16 Å in SDS and 5.88 Å in PFOS (Scheme 4e).

Interaction of catalyst precursor I1 with EDA in the micelles

In MD simulations, the cumulative count of atomic contacts between the reactant species at a reaction cutoff distance provides the frequency of the contacts to occur, and therefore the affinity of that particular contact.[40] Herein, to investigate the probability of the carbene insertion reaction

(from ethyl diazoacetate) to occur we calculated the cumulative count of atomic contacts between the catalyst **I1** and EDA molecules at a cutoff distance of 4.8 Å (see Supporting Information), in each surfactant model.[40] This distance has been chosen from previous DFT calculations for the intermediate in which the silver and the diazo compound interacts (Scheme 4f). To account for the proper orientation required for the reaction to occur, we performed the calculation specifically between the Ag atom and the diazo carbon of ethyl diazoacetate. The number of **I1**-EDA contacts after stabilization of the systems (after 400 ns of simulation) were 56 in SDS and 6 in PFOS (Scheme 4f and Figure S3). The larger number of interactions between the catalyst and the EDA molecules observed in the SDS seems reasonable, since both species were adsorbed on the surface of the micelles, remaining close enough to give the **I1**-EDA interaction. A detailed view of the interaction between **I1** and EDA molecules in a PFOS micelle during MD simulations is shown in the Supporting Video. In contrast, the **I1**-EDA interaction occurred to a lesser extent in PFOS since both species were found at different locations in the micelles; **I1** was inside the micelles, whereas the EDA molecules were placed on the micelles surface. It is worth mentioning that **I1** only exists in the first cycle, since the higher concentration of EDA and the partial solubility in water of the tetrahydrofuran disfavor the generation of **I1**, the unsaturated Tp^xAg moiety reacting with EDA en route to **I4** instead.

Moreover, it is well known that hydration shell may play a role in hindering the interactions between species in aqueous solvent. Thus, the presence of water in the first hydration shell around the Ag atom in **I1** was also monitored. As it is observed (Figure S3), when water molecules are around Ag, interactions with diazoacetate are not occurring. This demonstrates the ability of surfactants to, at least intermittently, isolate **I1** from the aqueous solvent, where the catalytic reaction does not occur.[23]

Molecular Dynamics simulation studies of the Intermediate I4

To gain further insights into the factors affecting the yields of the methane functionalization reaction with SDS and PFOS, we investigated in these two surfactants the methane trapping by the corresponding micelles as well as the interaction between methane molecules and **I4**, the silver-carbene intermediate. In the MD simulation of chemical reactions, interrupting the simulation and exchanging from a reactant version to a product version allows enforcing the corresponding changes in the topology of the system.[41] On this basis, we constructed two new **I4**-SDS and **I4**-PFOS systems, using as starting geometries the micelles resulting from the **I1** systems simulations (see Supporting Information). Therefore, the new built systems consisted of a water cubic box of $(100\ Å)^3$, with 208 molecules of the corresponding surfactant, i.e., SDS or PFOS, aggregated as micelles, 2 molecules of **I4** inside the PFOS micelles and adsorbed on the SDS micelles, and 2 molecules of tetrahydrofuran (Scheme 3b). We performed 100 ns MD simulations of the two new **I4** systems, at 300 K and 1 bar, to equilibrate them prior to methane introduction. The micellar phases remained stable in both systems, as shown by the Nclust, Nagg and SASA profiles (Figure S4). In agreement, the radial distribution function (g(r)) curves between surfactant headgroups and between surfactant headgroups and surfactants counterions were similar to those calculated for the **I1**-SDS and **I1**-PFOS systems (Figure S5). Only a decrease in the g(r) values of the largest peak between surfactants headgroups was observed in comparison with the **I1**-SDS and **I1**-PFOS systems (Scheme 3f and Figure S5), which could indicate that **I4**-SDS and **I4**-PFOS micelles are more separated from each other, leading to a decrease in the g(r) values.

We also analyzed the **I4**-micelles interactions. Interestingly, it is evident from visual inspection that the **I4** was adsorbed on the surface of both SDS and PFOS micelles along the MD simulations (Scheme 5a). This is in contrast with our previous results from **I1**-surfactant simulations, in which the **I1** was adsorbed only on the SDS micelles, whereas it was embedded in the PFOS micelles core (Scheme 4a). To confirm this finding, we calculated the

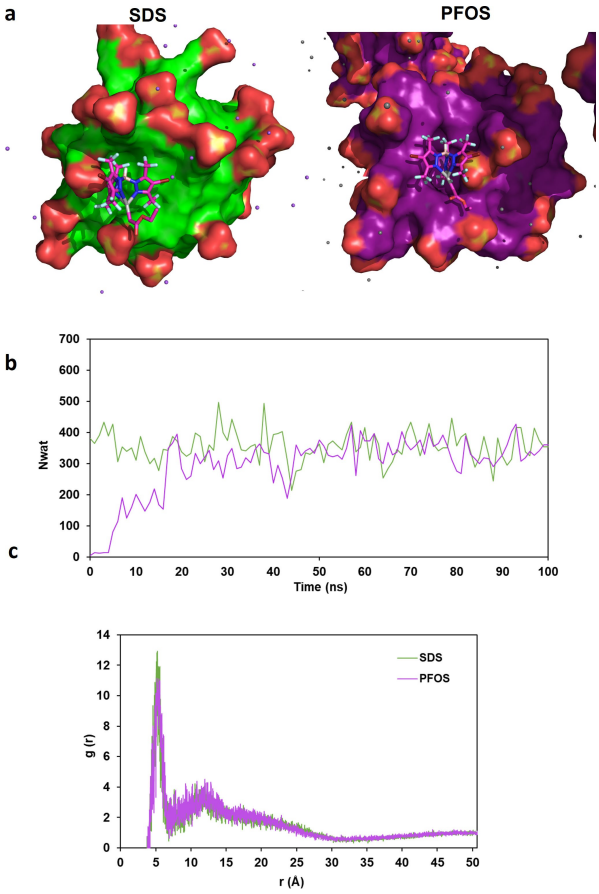

Scheme 5. MD simulation of intermediate **I4**. **a**, Molecular view of **I4** localization in the SDS and PFOS micelles. **b**, Number of water molecules surrounding the **I4**, within 10 Å of distance, over simulation time. **c**, Radial distribution, g(r), of the surfactant headgroups around **I4** molecules, in the MD simulations of the **I4**-SDS and **I4**-PFOS models. Water molecules and hydrogens are hidden for clarity.

number of water molecules (Nwat) around **I4** molecules. Values remained almost constant during the entire **I4**-SDS simulation, indicating that **I4** was stably adsorbed on the SDS micelles. However, the Nwat plot computed for PFOS showed an increase in the number of water molecules around the **I4**, along simulation time (Scheme 5b). Clearly, **I4** was expelled from PFOS micelles core, being more water exposed over time. We also monitored the radial distributions g(r) based on the probability densities of surfactants polar headgroups around the **I4** molecules (Scheme 5c). The largest intensity peaks were located at the same distance (5.17 Å) for both surfactants, and the g(r) curves were almost similar, in agreement with the same location of **I4** in the micelles of both surfactants. Nevertheless, the g(r) value of the largest peak is lower in PFOS than in SDS. The decrease could be due to the micelles that do not contain **I4** molecules, which are located farther away from the **I4** molecules in PFOS than in SDS.

Accumulation of I4 and methane in the SDS and PFOS micelles

Following the reaction path (Scheme 3a),[24] we introduced methane in the liquid phases of the **I4**-systems. According to experimental conditions, methane concentrations were 800 mM (482 molecules) in SDS, and 700 mM (425 molecules) in PFOS (Scheme 2b). The methane molecules were randomly distributed and the systems were simulated during 500 ns, at 300 K and 160 bar (experimental conditions).

The trajectories showed the migration of methane molecules from the bulk water towards the hydrophobic cores of the micelles (Scheme 6a and Figure S6A). Methane trapping was monitored by calculating the solvent accessible surface area, SASA, per methane molecule. Since the number of molecules initially introduced into the SDS and PFOS systems was different, SASA was computed and divided by the number of methane molecules, i.e., 482 in SDS and 425 in PFOS. Although methane internalization inside the micelles was confirmed by the 2D number-density maps for methane and surfactants (Figure S6B), different behavior was detected in each system. As shown in Scheme 6b, methane trapping in SDS occurred progressively, starting at 100 ns of simulation, while in the case of PFOS, methane trapped in the micelles remained constant up to 400 ns of simulation. Then, after 400 ns, maximum methane trapping was observed in both systems. To characterize the methane trapping inside the micellar interior, we computed the g(r) of surfactants tails around methane molecules (Scheme 6c). Clearly, the density was higher in PFOS than in SDS, suggesting higher affinity of the methane molecules to the inner cores of PFOS micelles as compared with SDS micelles (see Figure S8).

We have also investigated the dynamics and structures of the SDS and PFOS micelles in presence of methane by computing the SASA of the surfactants, the Nclust and the Nagg. The results were compared to the simulations without methane present. The degree of packing of the micelles was reduced in the presence of methane, as inferred from the increase of SASA values compared to those calculated in the absence of methane (average SASA of $4.68\times10^4\pm6.54\times10^2$ in SDS without methane versus $5.68\times10^4\pm9.67\times10^2$ with methane, and $4.16\times10^4\pm8.37\times10^2$ in PFOS without methane versus $5.13\times10^4\pm7.00\times10^2$ with methane) (Scheme 6d and 3e). Remarkably, SASA profiles of methane and surfactant molecules exhibited the same trend in each system. A slightly progressive decrease was observed in SDS over 100 ns of simulation time. On the other hand, a sharp decrease was detected in PFOS values at 400 ns (Scheme 6d). In addition, the number of micelles decreased in both systems when methane trapping occurred. At the beginning of the simulations, both systems exhibited 8 micelles. Afterwards, this number was reduced to 7 at 100 ns of simulation in SDS, and to 6 at 400 ns in PFOS (Scheme 6e). Because of that, the average number of surfactant monomers per micelle, Nagg, increased (Scheme 6f), i.e., larger micelles were formed during the absorption of methane. The net effect is that methane trapping results in changes in the structure and organization of the micelles, as well as in the degree of packing of the surfactant molecules.

Regarding the behavior of **I4**, it was observed that their molecules remained on the surface of the micelles. The number of water molecules surrounding the **I4**, Nwat, was almost constant during the simulations, confirming that the **I4** was stably adsorbed on the SDS and PFOS micelles (Scheme 6d and Figure S7A). Moreover, the radial distribution function (g(r)) curves of surfactant headgroups surrounding the **I4** molecules were similar to those calculated in the absence of methane. Only a decrease in the g(r) values of the largest peak was observed in comparison with the **I4**-SDS and **I4**-PFOS systems in absence of methane (Scheme 6c and Figure S7B), which could indicate that micelles were more separated from each other. Therefore, the behavior of **I4** was not modified by the presence of methane.

Interaction of I4 with methane in the micelles

Finally, we analyzed the interaction of **I4** with methane in the **I4**-SDS and **I4**-PFOS models. Since the highest methane accumulation occurred in the last 100 ns of simulation in both surfactants, we monitored the number of interactions between **I4** and methane during this period of the trajectories. The cumulative count of atomic contacts between both species, at a cutoff distance of 3.2 Å (see Supporting Information), between C atom coordinated to the silver in **I4** and any H of methane, was 48 in SDS, and 63 in PFOS (Scheme 6g and Figure S9). Since in both surfactants, SDS and PFOS, methane was internalized into the micelles, and the **I4** molecules remained at the surface of the micelles, we wondered whether water molecules could interfere with the **I4**-methane interactions. As observed in Figure S9, although there are some isolated water molecules in the first hydration shell of the intermediate, they do not interfere in the **I4**-methane interactions.

It is evident that more interactions occurred between **I4** and methane in PFOS than in SDS. Considering the higher

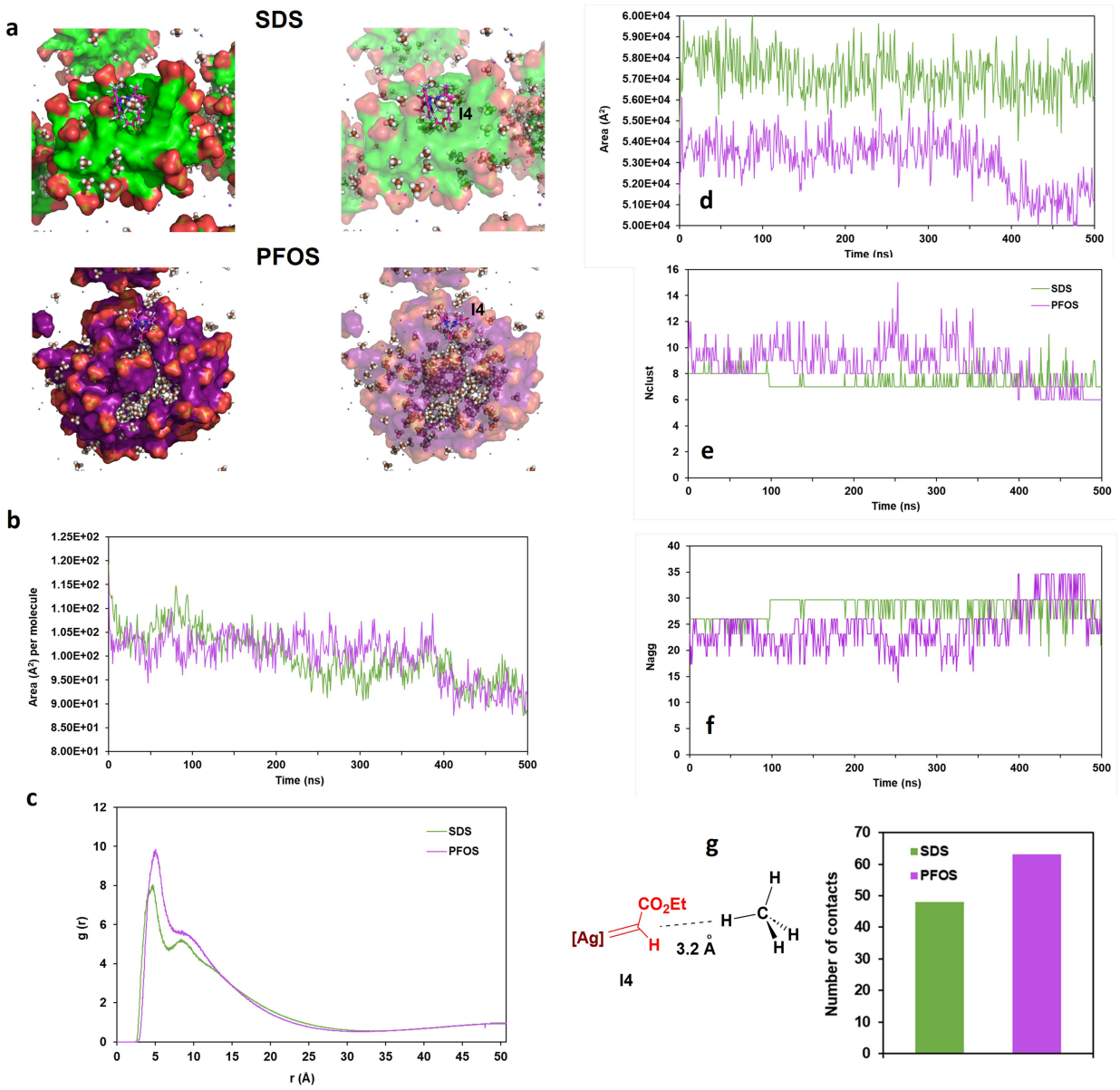

Scheme 6. Accumulation of **I4** and methane in the SDS and PFOS micelles. **a**, Atomic detail of the methane trapping inside the SDS and PFOS micelles, and **I4** localization in the micellar aggregates. **b**, Solvent accessible surface area (SASA) of methane per number of methane molecules, monitored along MD simulation time (t = 500 ns). **c**, Radial distribution, g(r), of the surfactant tails around the methane molecules, in the **I4**-SDS and **I4**-PFOS models. Water molecules and hydrogens are hidden for clarity, with the exception of methane hydrogens. **d**, Solvent accessible surface area (SASA) of surfactant molecules with methane computed over MD simulation time (t = 500 ns). **e**, Number of clusters, Nclust. **f**, Average number of surfactants monomer per cluster, Nagg, observed during the MD simulations (t = 500 ns) of the **I4** with SDS and PFOS model systems in presence of methane. **g**, Total number of interactions between **I4** and methane molecules, as computed for the last 100 ns of simulation time in the SDS and PFOS models.

affinity of methane for PFOS, and that PFOS formed a lower number of micelles (Nclust), it could be suggested that the number of methane molecules trapped per micelle is higher in PFOS, than in SDS. Moreover, in PFOS, the **I4** molecules are located in the micelles containing the highest concentration of methane, unlike what was observed in SDS, in which the micelles with the highest number of methane molecules in their interior do not harbor the catalyst (Scheme 6d–f and Figure S6).

General comments from MD simulations

Our computational studies have allowed the study of combination of different parameters involved in the complex phenomenon of formation and behavior of the micelles in the catalytic reaction, such as micelle stability, or the local distribution of reactants, among others. Although we cannot derive a direct relationship between these factors and the catalytic reaction outcome, our computational studies provide a solid explanation of the mechanism behind the

reported catalytic reaction, showing how the surfactants and their interactions with the reactants and the catalyst play a crucial role in the reaction outcome. Altogether, three blocks can be differentiated in this study (Scheme 7): surfactant aggregation, the micelles-**I1**-EDA system and the micelles-**I4**-methane system.

Surfactant aggregation. The studied surfactants spontaneously generate micelles in water, with SDS forming more stable aggregate, a feature also extended to micelle stability.

*Micelles-**I1**-EDA.* Aggregates interact with the catalyst precursor **I1**, albeit at different locations. **I1** molecules were buried inside the micelles core of PFOS and adsorbed on the SDS micelles surface. EDA molecules remained on the surface of both surfactants micelles. The number of contacts between the **I1** and EDA was higher in SDS than in PFOS.

*Micelles-**I4**-methane.* Methane accumulation was also investigated, showing a higher affinity of the methane molecules to the inner cores of PFOS micelles. Interestingly, methane accumulation resulted in changes in the structure and organization of the SDS and PFOS micelles, which appeared larger and less packed. **I4** was stably adsorbed on the surface of the SDS and PFOS micelles along the MD simulations. It is of note that regarding the number of interactions between **I4** and methane, those in PFOS were higher than the corresponding in SDS.

How do the MD studies fit into the experimental reactivity? Data collected indicate that the stability of the micelles formed from SDS allows to accommodate reactants and catalyst in the concentration, architecture, and time required for the catalytic reaction. Moreover, SDS provides the larger number of **I1**-EDA interactions, a reasonable finding since both species were adsorbed on the surface of the micelles, resulting in very high local concentrations of catalyst and reactants. On the other hand, PFOS provides fewer stable micelles compared to SDS, and showed a lower number of **I1**-EDA interactions. Despite that, the catalytic reaction reaches a 14% yield when using PFOS. This is explained as the result of the high affinity of methane for the inner PFOS micellar space, and the higher number of contacts produced between **I4** and methane in this surfactant compared to SDS.

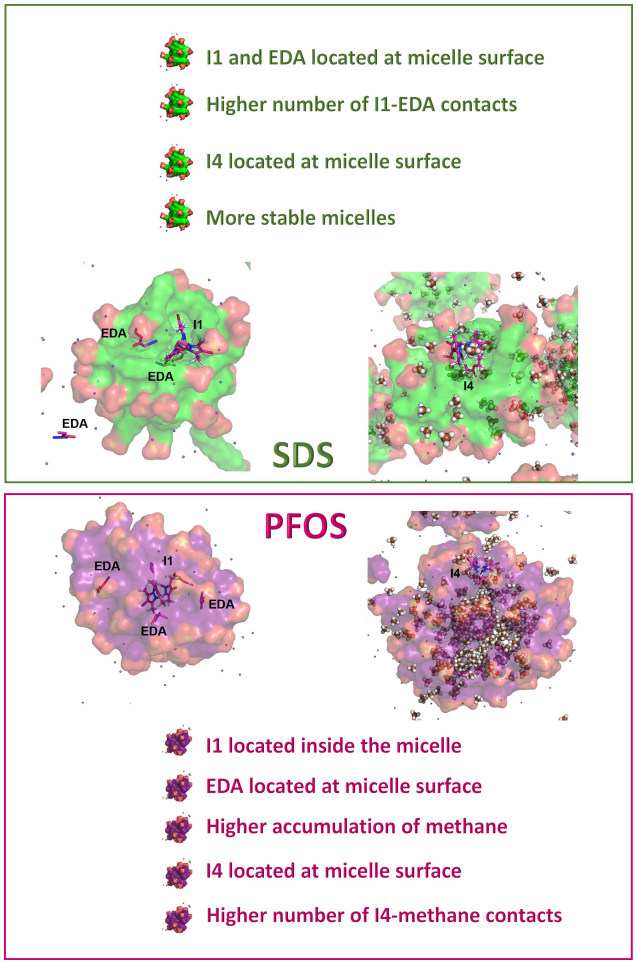

Scheme 7. Global results for the MD simulations of the methane functionalization in micellar media.

Conclusion

We report herein the first in depth time-evolution study by Molecular Dynamics (MD) simulations on the methane catalytic functionalization in a micellar aqueous media. Data obtained allows explaining the experimental results, providing explanations of micelle formation, the accommodation of the catalyst (in two of its different species along the catalytic cycle), the diazo compound and methane within the micellar media and the intermolecular collisions leading to the product. Our computational studies also highlight the unique role of the studied surfactants (SDS, PFOS) in the reaction. The simulations allow to ascertain the structural properties of the formed micelles, and the relative distribution of the main reactants and the relationship among them, and how these factors impact the assembly, the molecular collisions and ultimately lead to the catalytic reaction. The vision of MD simulations to provide reliable, quantitative, and mechanistic predictions of catalytic reactions in micellar media is now a reality and will open new opportunities for advancing in the development and optimization of catalytic micellar systems, reducing both the time and the cost of the experimentation.

Supporting Information

The authors have cited additional references within the Supporting Information (Ref. [42–56]).

Acknowledgements

We thank to Ministerio de Ciencia e Innovación for Grants PID2020-113797RB-C21, PID2020-113588RB-I00, and PRE2018-086249, also funded by FEDER "Una manera de hacer Europa". We also thank Junta de Andalucía (P18-1536RT) and Universidad de Huelva (P. O. Feder UHU-

202024). Funding for open access is given by Universidad de Huelva/CBUA.

Conflict of Interest

The authors declare no conflict of interest.

Data Availability Statement

The data that support the findings of this study are available in the supplementary material of this article.

Keywords: Carbene Transfer in Micelles · Methane Functionalization · Micellar Catalysis · Molecular Dynamics Simulations · Organometallic Catalysis

[1] P. T. Anastas, J. C. Warner, *Green Chemistry: Theory and Practice*, Oxford University Press, New York, **1998**.
[2] F. P. Byrne, S. Jin, G. Paggiola, T. H. M. Petchey, J. H. Clark, T. H. Farmer, A. J. Hunt, C. R. McElroy, J. Sherwood, *Sustain. Chem. Process.* **2016**, *4*, 7, https://doi.org/10.1186/s40508-016-0051-z.
[3] P. T. Anastas, M. M. Kirchhoff, T. C. Williamson, *Appl. Catal. A* **2001**, *221*, 3–13.
[4] J. Kooroshy, R. P. Meindersma, M. Rademaker, T. Sweijs, A. Diederen, M. Beerthuizen, S. de Goede, In *Scarcity of Minerals–A strategic security issue.* The Hague Centre for Strategic Studie. **2010**, *2*, 1.
[5] M. Cortes-Clerget, N. Akporji, J. Zhou, F. Gao, P. Guo, M. Parmentier, F. Gallou, J.-Y. Berthon, B. H. Lipshutz, *Nat. Commun.* **2019**, *10*, 2169.
[6] M. Cortes-Clerget, J. Yu, J. R. A. Kincaid, P. Walde, F. Gallou, B. H. Lipshutz, *Chem. Sci.* **2021**, *12*, 4237–4266.
[7] B. H. Lipshutz, S. Ghorai, *Green Chem.* **2014**, *16*, 3660–3679.
[8] B. H. Lipshutz, S. Ghorai, *Aldrichimica Acta* **2012**, *45*, 3–16.
[9] B. H. Lipshutz, S. Ghorai, *Aldrichimica Acta* **2008**, *41*, 59–72.
[10] B. H. Lipshutz, N. A. Isley, J. C. Fennewald, E. D. Slack, *Angew. Chem. Int. Ed.* **2013**, *52*, 10952–10958.
[11] F. Gallou, N. A. Isley, A. Ganic, U. Onken, M. Parmentier, *Green Chem.* **2016**, *18*, 14–19.
[12] A. M. Linsenmeier, W. M. Braje, *Tetrahedron* **2015**, *71*, 6913–6919.
[13] a) N. J. Buurma, *Annu. Rep. Sect. B Org. Chem.* **2012**, *108*, 316–333; b) L. S. Romsted, C. Bravo-Díaz, *Curr. Opin. Colloid Interface Sci.* **2013**, *18*, 3–14.
[14] M. P. Andersson, F. Gallou, P. Klumphu, B. S. Takale, B. H. Lipshutz, *Chem. Eur. J.* **2018**, *24*, 6778–6786.
[15] M. P. Andersson, *J. Colloid Interface Sci.* **2022**, *628*, 819–828.
[16] S. Das, S. Paul, *J. Phys. Chem. B* **2015**, *119*, 3142–3154.
[17] Y. R. E. Silva, J. R. Grigera, *RSC Adv.* **2015**, *5*, 70005–70009.
[18] G. M. C. Silva, P. Morgado, P. Lourenço, E. J. M. Filipe, *Proc. Natl. Acad. Sci. USA* **2019**, *116*, 14868–14873.
[19] T. Taddese, R. L. Anderson, D. J. Bray, P. B. Warren, *Curr. Opin. Colloid Interface Sci.* **2020**, *48*, 137–148.
[20] M. Z. Dehagani, F. Yousefi, F. Seidi, B. Bagheri, A. H. Mashhadzadeh, G. Naderi, A. Esmaeli, O. Abida, S. Habibzadeh, M. R. Saeb, M. Rybachuk, *Sci. Rep.* **2021**, *11*, 18753.
[21] K. Farah, F. Müller-Plathe, M. C. Böhm, *ChemPhysChem* **2012**, *13*, 1127–1151.
[22] Y.-M. Huang, W. You, B. G. Caulkins, M. F. Dunn, L. J. Mueller, *Protein Sci.* **2016**, *25*, 166–183.
[23] R. Gava, P. Ballestín, A. Prieto, A. Caballero, P. J. Pérez, *Chem. Commun.* **2019**, *55*, 11243–11246.
[24] A. Olmos, R. Gava, B. Noverges, D. Bellezza, K. Jacob, M. Besora, W. M. C. Sameera, M. Etienne, F. Maseras, G. Asensio, A. Caballero, P. J. Pérez, *Angew. Chem. Int. Ed.* **2018**, *57*, 13848–13852.
[25] A. Caballero, E. Despagnet-Ayoub, M. M. Díaz-Requejo, A. Díaz-Rodríguez, M. E. González-Núñez, R. Mello, B. K. Muñoz, W. Solo Ojo, G. Asensio, M. Etienne, P. J. Pérez, *Science* **2011**, *332*, 835–838.
[26] H. L. Clever, C. L. Young, Eds, *IUPAC Solubility Data Series, Vol. 27/28, Methane*, Pergamon Press, Oxford, England, **1987**.
[27] X.-H. Liu, X.-H Luo, S.-X. Lu, J.-C. Zhang, W.-L Cao, *J. Colloid Interface Sci.* **2007**, *307*, 94–100.
[28] H. Schott, *J. Colloid Interface Sci.* **1997**, *192*, 458–462.
[29] D. N. LeBard, B. G. Levine, P. Mertmann, S. A. Barr, A. Jusufi, S. Sanders, M. L. Klein, A. Z. Panagiotopoulos, *Soft Matter* **2012**, *8*, 2385–2397.
[30] D. Yordanova, I. Smirnova, S. Jakobtorweihen, *J. Chem. Theory Comput.* **2015**, *11*, 2329–2340.
[31] K. Schäfer, H. B. Kolli, M. K. Christensen, S. L. Bore, G. Diezemann, J. Gauss, G. Milano, R. Lund, M. Cascella, *Angew. Chem. Int. Ed.* **2020**, *59*, 18591–18598.
[32] W. Wang, W. Lu, L. Jiang, *J. Phys. Chem. B* **2008**, *112*, 1409–1413.
[33] A. J. M. Valente, H. D. Burrows, S. M. A. Cruz, R. F. P. Pereira, A. C. F. Ribeiro, V. M. M. Lobo, *J. Colloid Interface Sci.* **2008**, *323*, 141–145.
[34] L. G. Chen, H. Bermudez, *Langmuir* **2012**, *28*, 1157–1162.
[35] T. Shoaib, J.-M. Ha, Y. Han, W.-R. Chen, C. Do, *Phys. Chem. Chem. Phys.* **2022**, *24*, 16988–16996.
[36] S. Prévost, M. Gradzielski, *J. Colloid Interface Sci.* **2009**, *337*, 472–484.
[37] B. Tah, P. Pal, M. Mahato, G. B. Talapatra, *J. Phys. Chem. B* **2011**, *115*, 8493–8499.
[38] H. Ishkhanyan, N. H. Rhys, D. J. Barlow, M. J. Lawrence, C. D. Lorenz, *Nanoscale* **2022**, *14*, 5392–5403.
[39] G. Kacar, *Colloid Polym. Sci.* **2019**, *297*, 1037–1051.
[40] K. Farah, F. Müller-Plathe, M. C. Böhm, *ChemPhysChem* **2012**, *13*, 1127–1051.
[41] M. Biedermann, D. Diddens, A. Heuer, *J. Chem. Theory Comput.* **2021**, *17*, 1074–1085.

Manuscript received: October 3, 2023
Accepted manuscript online: December 6, 2023
Version of record online: January 11, 2024